



Research Article

Thermal and electrical characterization of composite metal oxides particles from periwinkle shell for dielectric application

A. A. Abdelmalik¹ · A. Sadiq¹

© Springer Nature Switzerland AG 2019

Abstract

Rather than synthesizing metal oxides through chemical processes as fillers in polymer composites, metal oxides from natural sources (waste) could provide a cheaper and environmentally friendly alternative. In this work, a fine powder prepared from properly cleaned periwinkle shells was examined for its use as filler for polymer composites for high-voltage application. The powder was characterized using scanning electron microscopy (SEM), X-ray fluorescence spectrometry, Fourier transform infrared spectroscopy, thermal conductivity set-up and a programmable LCR Bridge. The SEM image of the powder revealed a range of particle sizes that vary from 2 to 34 μm . The chemical analysis shows that CaO is the dominant metal oxide in the powder with 81.8 wt%. The dielectric constant and the electrical conductivity of the powder are 11.08 and $1.5876 \times 10^{-8} \text{ S m}^{-1}$, respectively, at the frequency of 200 Hz. The electrical conductivity of the powder is lower than the conductivity of pure CaO, while the thermal conductivity is slightly higher than that of pure CaO. This could be due to the influence of the other constituent metal oxides. This is an indication that periwinkle shell powder if properly processed to micro- and even nano-sized particles can be a good candidate as a filler in polymer composites to produce polymeric insulation with good insulating and thermal conducting properties.

Keywords Animal waste · Periwinkle shell · Calcium oxide · Composite insulator · Polymeric insulation

1 Introduction

Metal oxide micro- and nanoparticles are important materials due to their applications in several areas such as catalysis, sensors, optoelectronic materials and environmental remediation [1]. In a quest for polymeric insulation with improved dielectric and electrical properties, metal oxide particles in micro- and nano-sized were also found to have played a vital role. Polymer nanocomposites were found to have improved the dielectric loss and breakdown strength at certain filler content. Some of the common metal oxides used to modify the structure of the polymer matrix include SiO_2 , TiO_2 and Al_2O_3 [2, 3]. While the microparticles of these metal oxides produced materials with increased dielectric loss, the nanoparticles were found to produce polymer composites with decreasing dielectric loss at lower

filler loading. This was attributed to the morphology of the nano-materials [3].

Calcium oxide as an alkaline earth metal oxide is known to have many applications. This includes its use as catalyst [4], toxic-waste remediation agent, an additive in refractory [5, 6], a crucial factor for CO_2 capture [7–9], flue gas desulphurization and pollutant emission control [10]. It has also been used as an additive to modify the electrical and dielectric properties of materials [11]. In a study to improve the mechanical, thermal and processability properties of recycled polyethylene terephthalate/polyethylene mixture (70 wt/30 wt%), CaO nanoparticles were added to the mixture. The thermal stability was reported to be pronounced with the addition of CaO, the hardness of the mixtures increased progressively with the increase in CaO [12]. In another work to study the effect of CaO

✉ A. A. Abdelmalik, aaabdelmalik@gmail.com; A. Sadiq, sadiqabdulrahman99@gmail.com | ¹Department of Physics, Ahmad Bello University, Zaria, Nigeria.



SN Applied Sciences (2019) 1:373 | <https://doi.org/10.1007/s42452-019-0388-5>

Received: 24 December 2018 / Accepted: 20 March 2019 / Published online: 28 March 2019

SN Applied Sciences
A SPRINGER NATURE journal

nanoparticles on the properties of polyamide 6, it was reported that there was a notable improvement in the thermal stability of the nanocomposites compared with neat polyamide 6. [13]. CaO nanoparticles are often produced via thermal treatment of Ca(OH)_2 [11, 14] or CaCO_3 [7, 15] as precursors. They have also been prepared by calcination of Ca(OH)_2 which was synthesized by adding NaOH [1]. A report on the electrical properties of calcium oxide shows that the metal oxide has an electrical conductivity of $1 \times 10^{-6} \text{ S m}^{-1}$ [16, 17]. The electrical conductivity of polyaniline (PANI) nanofibers was studied by systematically varying the addition of CaO in the range from 0.005 to 1.00 g. The obtained result shows that the highest conductivity value of 6.329 S cm^{-1} was obtained by the addition of the lowest amount of CaO (0.005 g). Increase in CaO loadings was reported to have resulted in a decrease in the electrical conductivity of the composite material [18].

Aside from clay, other micro- and nanoparticles are synthesized using several methods, and the controlled production of metal oxide nanoparticles is important for its effective and successful application [11, 19, 20]. Animal shells are known to be composed of several metal oxides that are being exploited for numerous industrial applications. Instead of producing micro- or nanoparticle through chemical methods, can the micro- or nanoparticles produced from such waste sea animal shells serve the same purpose? The report of the characterization of natural pearl of *Pinctada fucata* from Gulf of Mannar using scanning electron microscope (SEM), and energy dispersive studies (EDS) revealed that natural pearl contained Ca and O in the form of calcium oxide and Nb was present. They suggested that this may be the reason for the formation of lustrous layer in the shell [21]. Cockleshell was reported to consist of a higher percentage of calcium carbonate. Kamba et al. attempted to synthesize calcium carbonate nanocrystal from cockleshell powder using high-pressure homogenizer. The synthesized CaCO_3 was reported to be composed of the aragonite form of calcium carbonate. Tamasan et al. attempted to produce hydroxyapatite and/or tricalcium phosphate (TCP) from Sputnik sea urchin shells—*Phyllacanthus imperialis* and

from a type of sea snail shell called *Trochidae Infundibulum concavus* [22]. The FTIR analysis revealed the presence of carbonate groups of CaCO_3 identified from the peaks in the region of $1400\text{--}1600 \text{ cm}^{-1}$ of the spectra. The materials formed after the chemical reaction with H_3PO_4 were reported to be promising materials for bone fillers [23]. Periwinkle is another type of seashell animal. It is a species of small edible sea snail that is consumed in large quantity in Nigeria. Its consumption produces residual shells which posed an environmental hazard. The shell is a natural ceramics which contained several metal oxides used in material applications such as a filler in concrete production. The shell ash was investigated as a replacement for cement in concrete. In this work, microparticles prepared from waste periwinkle shells are characterized for its possible use in polymer composite for high-voltage electrical insulation application.

2 Materials and methods

Periwinkle shells are shown in Fig. 1a, obtained from the local market in Zaria, Nigeria, which were properly washed with water and followed by acetone. The washed shells were dried in an oven for 24 h. The cleaned periwinkle shells were passed through a turning operation in a crusher and ball milling machine to produce the powder. The crushed particles were sieved using a sieve of $75 \mu\text{m}$ mesh size to produce the powder shown in Fig. 1b. A pellet of diameter 40 mm and thickness 2 mm was prepared from the periwinkle shell powder. Cellulosic resin was added to the powder as a binder and was then carefully mixed. The mixture was pressed into a pellet using a hydraulic press by applying four tonnes load for 120 s. The microstructure of the samples was studied using Phenom ProX Desktop scanning electron microscope (SEM) equipped with an energy dispersive spectroscopy system. The samples were held on the sample holder using a double-sided carbon tape before putting them inside the sample chamber, and SEM was operated at an accelerating voltage of 15 kV, and the image was recorded.



Fig. 1 Samples **a** periwinkle shell, **b** periwinkle shell powder and **c** periwinkle shell pellet

Agilent Cary 630 FTIR machine was used to identify the chemical constituents in the compound from the characteristic frequencies on the spectra. And the elemental composition of the powder was determined using Oxford X-Supreme 8000 X-ray fluorescence (XRF) spectrometer. The powder obtained from the periwinkle shells was loaded in the sample chamber of the spectrometer at an accelerating voltage of 30V and current of 10 mA to produce the X-rays to excite the sample for 10 min. The fluorescent X-rays emitted by the material sample are directed into a solid-state detector which produced a continuous distribution of pulses, the voltages of which are proportional to the incoming photon energies, and the diffraction grating used is usually a single crystal, the angle of incidence and take-off on the crystal, a single X-ray wavelength was selected. The counter is a chamber containing a gas that is ionized by X-ray photons and the signal is amplified, transformed into an accumulating digital count. The system is controlled by a PC running the dedicated Mini Pal analytical software.

The thermal conductivity of the pelletized powder was determined using Searle's method. The set-up was initially used to determine the thermal conductivity of materials with known thermal conductivity. The pelletized sample was placed in the sample chamber and heated at one end by the means of an electrical power supply. Water was made to flow through the apparatus and it entered the tube at the end of the steam chamber and leaves at the end nearer to it. The power supply was switched on when the water was flowing, and the input current and voltage were recorded. The water starts to get hotter until a constant temperature difference is reached, and the water flow was adjusted so that the temperature difference is about 5 °C. Thermometers θ_1 and θ_2 placed where water was coming in and out were used to measure the temperatures of the outlet and inlet water. The temperatures θ_1 and θ_2 were recorded. The experiment was repeated three times to determine the average value of the thermal conductivity of the sample.

The pelletized powder was placed in a two-electrode test cell in a temperature-controlled chamber for dielectric measurement. The terminals of the test cell were connected to Rohde and Schwarz HM8118 Programmable LCR Bridge with frequencies range of 20 Hz to 200 kHz as shown in Fig. 2. It has a measurement accuracy of 0.05%. The set-up was used to measure the capacitance, loss tangent and the resistance of the sample at a temperature from 25 to 80 °C.

3 Results and discussions

Figure 3 shows the scanning electron microscopy (SEM) image of the periwinkle shell powder particles. The image revealed a surface of random-sized particles. The particles'



Fig. 2 Dielectric measurement test set-up

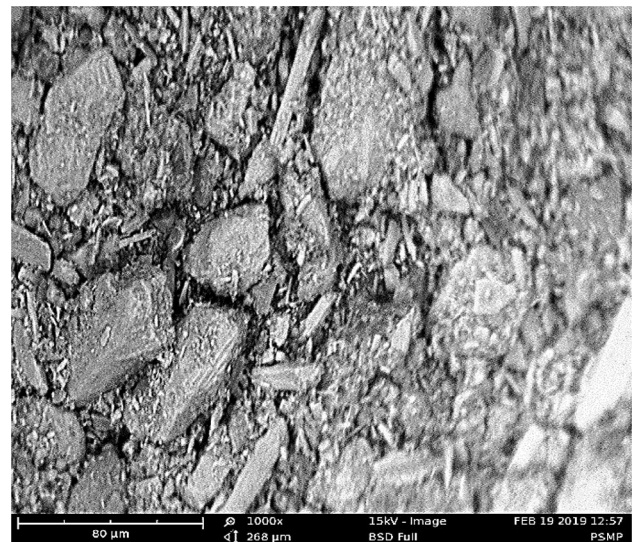


Fig. 3 SEM microstructure of periwinkle shell powder at the magnification of $\times 1000$

average sizes were determined from the micrograph. The periwinkle shell powder was found to have particle sizes that range from 2 to 34 μm .

Figure 4 shows the FTIR spectra of the periwinkle shell powder. The weak band at 1785.4 cm^{-1} corresponds to C=O bonds from carbonate. There appeared two well-defined infrared peaks at 1468.6 and 857.3 cm^{-1} which are attributed to the characteristic C–O stretching and bending modes of calcium carbonate, respectively. The sharp peak at 711.9 cm^{-1} which appeared at the fingerprint region is related to Ca–O bonds. The observed band at 1080.9 cm^{-1} is assigned to the symmetric stretching of CO_3^{2-} ions. The peak is an indication that the shell composed of the aragonite form of calcium carbonate. The peak at 1785.4 cm^{-1} is among the common characteristic features of the carbonate ions in calcium carbonate. The 1036.2 cm^{-1} may be related to the presence of Si–O bonds [21, 22, 24].

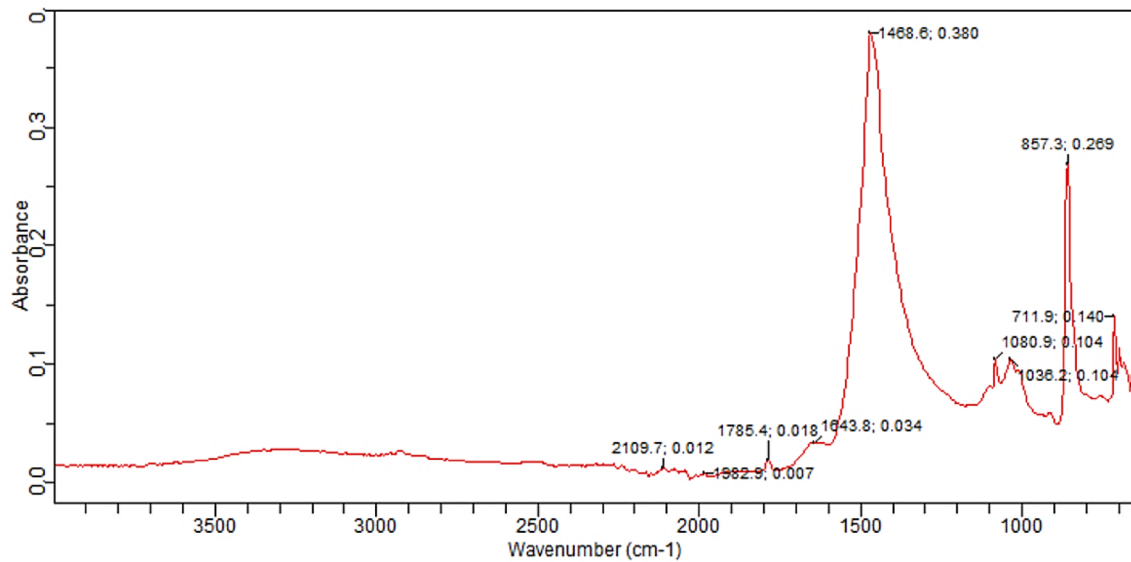


Fig. 4 FTIR spectra of periwinkle shell powder

Figure 5 shows the XRF spectra of periwinkle shell powder. There appeared two peaks (3.71 and 4.02 keV) on the spectra that are assigned to calcium. The 3.71 keV peak has the highest intensity, an indication that calcium is the dominant metal in the sample. Other visible peaks are at 1.71 keV assigned for silicon, 1.22 keV for

magnesium, 1.42 keV for aluminium, 6.41 keV for iron and 2.2 keV for sulphur [25]. The determined chemical composition of the periwinkle shell powder from the spectra analysis as presented in Table 1 shows a high amount of calcium oxide. This is associated with the presence of calcium carbonate, the main component of

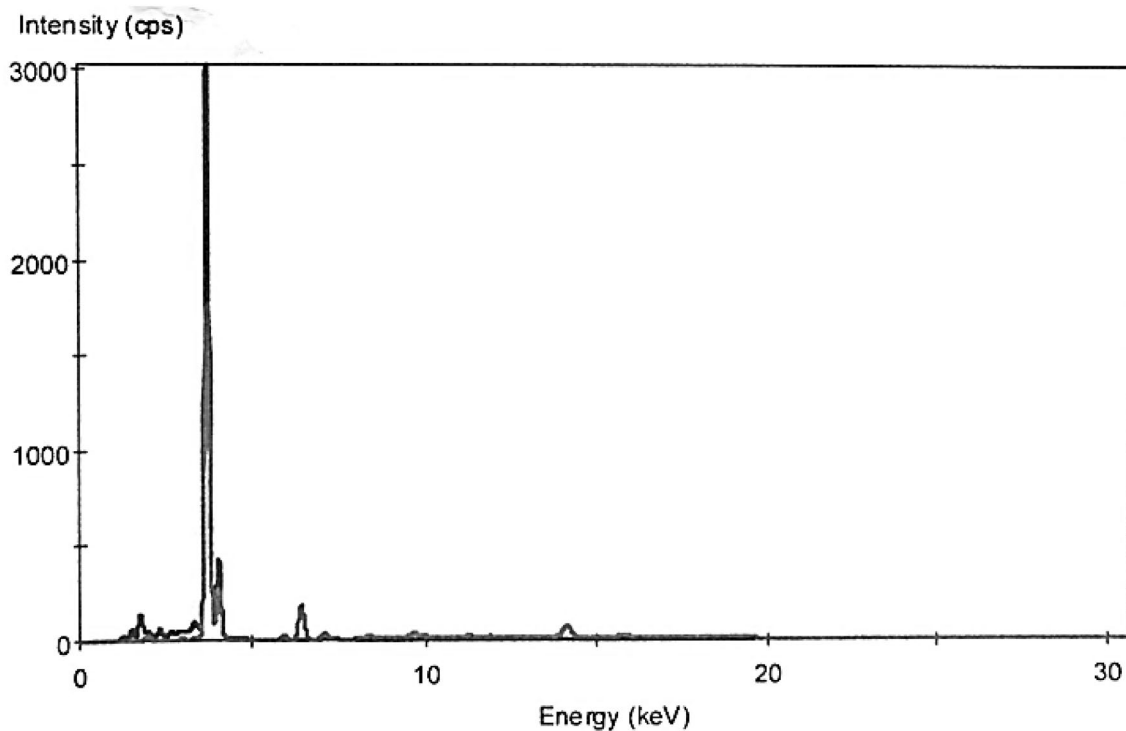


Fig. 5 XRF spectra of periwinkle shell powder

Table 1 Chemical composition of calcium carbonated periwinkle shell powder by XRF

Oxide	Concentration (wt%)
Na ₂ O	0.002
MgO	3.069
Al ₂ O ₃	2.548
SiO ₂	6.734
P ₂ O ₅	0.752
SO ₃	1.001
Cl	0.280
K ₂ O	0.295
CaO	81.803
TiO ₂	0.147
Cr ₂ O ₃	0.036
Mn ₂ O ₃	0.437
Fe ₂ O ₃	2.380
ZnO	0.010
SrO	0.508

the powder as revealed by the FTIR results. The shell contained traces of several oxides of metals such as sodium oxide (Na₂O), phosphorous oxide (P₂O₅), titanium oxide (TiO₂), chromium oxide (Cr₂O₃) and zinc oxide (ZnO) with calcium oxide (CaO) as the dominant metal oxide with a concentration of about 81.8%.

The elemental analysis shows that CaO has the highest compositions in the periwinkle shell powder and it constitutes about 81.8% of the total elemental composition. SiO₂, MgO, Al₂O₃, Fe₂O₃ and SO₃ constitute about 15.732% of the elemental composition. CaO, SiO₂, Fe₂O₃, Al₂O₃, TiO and MgO are among the hardest substances. Traces of P₂O₅, SrO, Mn₂O₃, K₂O, Cl, Cr₂O₃ and ZnO were also found to be present. The elemental composition has similarity with XRF analysis of clay which has been used in polymer matrix composite but with 48.12% SiO₂ and 34.54% Al₂O₃ [26].

The thermal conductivity, K of the sample, was obtained with the relation:

$$K = \frac{VIL}{A(\theta_2 - \theta_1)} \quad (1)$$

where V is voltage, I is the current flowing through the sample, A is the cross-sectional area of the sample, θ_1 is the temperature of inlet water, θ_2 is the temperature of outlet water and L is the thickness of the sample. The experimental measurement was repeated three times, and the variables were recorded, and the thermal conductivity values were calculated to be 16.884553, 20.121950, 16.884553 Wm⁻¹ k⁻¹, respectively. The average thermal conductivity, K of the sample, was calculated to be 17.963685 Wm⁻¹ k⁻¹.

Materials of good thermal conductivity are used as electrical insulation as they perform a dual function of insulant and coolant. They are supposed to serve as a medium to transport the heat generated due to ohmic heating in the electrical system. Thermal conductivity values of some of metals oxides are as follows: CuO has a thermal conductivity between 20 and 30 Wm⁻¹ k⁻¹, SiO₂ is 1.7 Wm⁻¹ k⁻¹, MgO is 35 Wm⁻¹ k⁻¹, Al₂O₃ is 35 Wm⁻¹ k⁻¹, TiO is 9.2 Wm⁻¹ k⁻¹ and CaO is 15 Wm⁻¹ k⁻¹ [27]. Periwinkle shell pellet has a thermal conductivity of 18.0 Wm⁻¹ k⁻¹ which is close to the thermal conductivity of pure CaO with a thermal conductivity of 15 Wm⁻¹ k⁻¹. The difference may likely be due to the presence of high thermal conductive metal oxides in the powder. The thermal conductivity is higher than that of TiO₂ and SiO₂. This is an indication that its dispersion in the polymer will produce a composite with better thermal conductive properties compared with the commonly used TiO₂ and SiO₂. The thermal conductivity of the sample is also slightly higher than that of pure CaO. This is an indication that the sample under study which contained 81.8% CaO is more thermally conducting compared with the pure CaO crystal.

The dielectric measurements were taken within the frequency range of 200 Hz to 50 kHz. Figures 6 and 7 present the relative permittivity (dielectric constant) and loss tangent of the samples from an ambient temperature of 25–80 °C. The relative permittivity was relatively constant for all temperature between the frequency ranges of 50–2 kHz. Below 2 kHz, a slight increase was observed in the relative permittivity. At room temperature, the relative permittivity (also known as dielectric constant) has an average value of 9.5 at higher frequency window. This increased to 11 at a frequency of 200 Hz. This value is comparable to the value of 12.2 obtained for CaO at 300 K [28]. Meanwhile, temperature increase led to an increase in the real part of the relative permittivity. The loss tangent

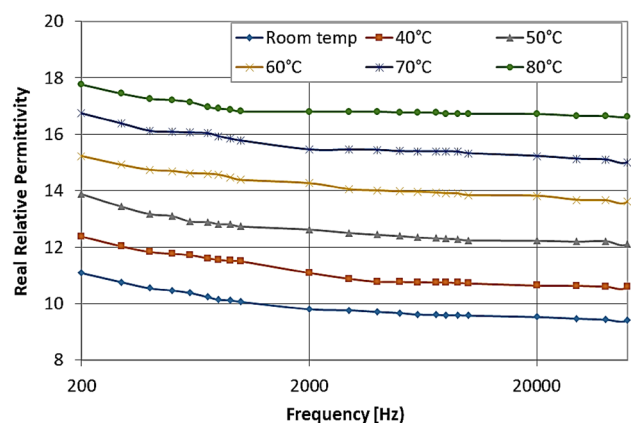


Fig. 6 Semi-log plot of real relative permittivity versus frequencies from 200 Hz to 50 kHz for different temperatures

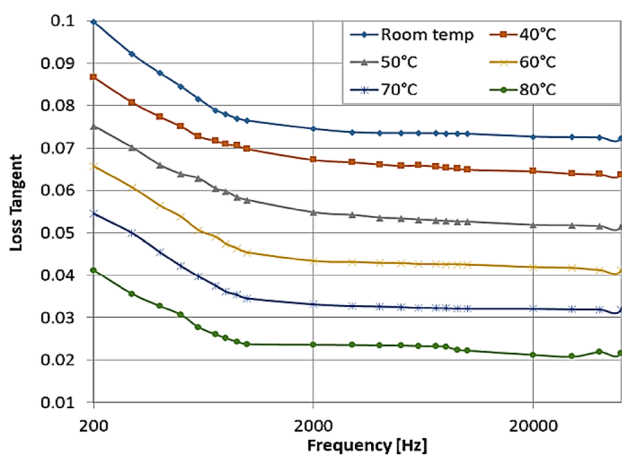


Fig. 7 Semi-log plot of loss tangent versus frequencies from 200 Hz to 50 kHz for different temperatures

(dielectric loss) was also observed to be relatively stable between 50 and 1 kHz, and an increase was observed in the permittivity below 1 kHz with a slope of about -1 . This is an indication of DC conduction mechanisms in the sample. Increase in temperature resulted in a decrease in the dielectric loss.

Application of electric field resulted in charge transport and orientation polarization of dipoles in the sample. The electric displacement, D that describes the influence of the applied electric field, E , on the distribution of charged particle motion and electric dipole reorientation, is expressed as [29]:

$$D(t) = \epsilon_0 \epsilon^* E_0 \exp(i\omega t) \tag{2}$$

The decrease in loss tangent with increasing frequency between 200 Hz and 1 kHz is an indication of pure DC conduction. The conductivity beyond 1 kHz is connected with AC conductivity which is a combination of DC conductivity and loss due to polarization. The DC conductivity is likely due to charge transport by electrons ‘hopping’ from donor to donor. It may also be due to negative oxygen ions migrating through the crystal.

When temperature increases, the system entropy increases and that will attempt to randomize the dipoles, thereby counteracting the effect of the applied electric effect. This leads to the reduction in charge transport and polarization and a reduction in the dielectric loss of the sample.

The log–log plot of electrical conductivity of the sample with frequency in Fig. 8 revealed an interesting feature. The conductivity was stable up to a certain frequency before it acquired a slope of about 1. The slope was nearly the same at all temperature. The motion of the charged particles in the dielectric material, besides causing conduction current, gives rise to the polarization of the dielectric material.

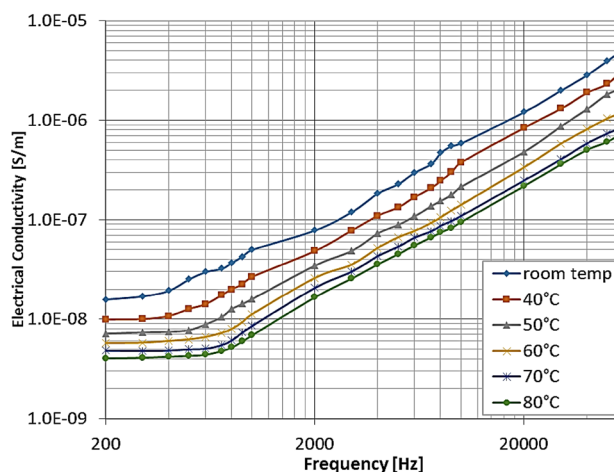


Fig. 8 Log–log plot of real electrical versus frequencies from 200 Hz to 50 kHz for different temperatures

If the total loss in the dielectric is visualized as a combination of DC conductivity and loss due to polarization, the measured dielectric loss, $\sigma(\omega)$, can be expressed as [29]:

$$\sigma(\omega) = \sigma_0 + \omega \epsilon_0 \epsilon''(\omega) \tag{3}$$

The constant part which is a DC conduction is attributed to charge transport, while the part with a slope is the AC conductivity which is attributed to both charge transport and loss due to polarization processes. The electrical conductivity decreases with an increase in temperature, and the turning point from DC to AC conductivity shifts towards higher frequency as temperature increases. This also showcases the influence of temperature on charge transport and polarization mechanism in the material. Temperature reduced the influence of polarization on the electrical conductivity of the sample thereby extending the frequency range of DC conductivity.

The DC conductivity values at 300 Hz were plotted in Arrhenius plot in Fig. 9 using the Arrhenius relation:

$$\sigma = A e^{\frac{E_a}{k_B T}} \tag{4}$$

where σ is electrical conductivity, k_B is the Boltzmann constant, T is the temperature in Kelvin, E_a is the thermal activation energy with the same unit as $k_B T$ and A is pre-exponential constant.

The plot shows that electrical conductivity fits into Arrhenius relation within the temperature range studied. The thermal activation energy was evaluated to be 0.236 eV. The thermal activation energy suggests the energy necessary for the electrons to ‘hop’ from one donor to another or the energy needed for negative oxygen ions to migrate through the crystal at low temperature.

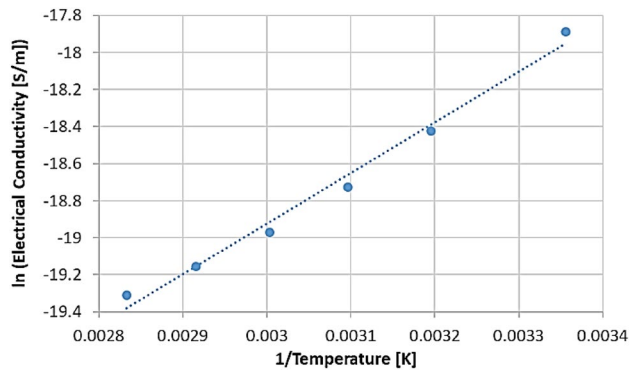


Fig. 9 Arrhenius plot for electrical conductivity

4 Conclusions

Metal oxide micro-composite powder was produced from the waste periwinkle shell. The micro-composite contained 81.8% CaO, 15.7% of the combination of MgO, Al₂O₃, SiO₂, SO₃, Fe₂O₃ and traces of some other metal oxides such as P₂O₅, P₂O₅, SO₃, TiO₂, Cr₂O₃, Mn₂O₃, SrO.

The powder has a thermal conductivity of 18.0 Wm⁻¹ k⁻¹, a value slightly higher than the thermal conductivity of pure CaO. The difference may be attributed to the presence of higher thermal conductive components in the powder. The thermal conductivity is higher than that of TiO₂ and SiO₂ that are commonly used as filler in polymeric insulation. This suggests that a polymer composite with the powder may produce insulating materials with better thermal conductive properties in comparison with polymer composites with TiO₂ and SiO₂. The relative permittivity (dielectric constant) of the pelletized powder is within the range of metal oxide ceramics. It increases with an increase in temperature. The loss tangent decreases with temperature. There exist an AC conductivity which is a combination of DC conductivity and loss due to polarization. The DC conductivity is likely due to charge transport by electrons 'hopping' from donor to donor. It may also be due to negative oxygen ions migrating through the crystal. The electrical conductivity of the powder is lower than the conductivity of pure CaO. This suggests that periwinkle shell powder if properly processed to micro- and even nano-sized particles can be a good candidate as a filler in polymers to produce polymeric insulation with good insulating and thermal conducting properties. The application of periwinkle shell in composite insulation materials will give new use to the animal waste.

Acknowledgements The authors wish to acknowledge the contribution of Mr. Muhammad Dabai towards setting up the thermal conductivity measurement facility.

Compliance with ethical standards

Conflict of interest The authors declare that they have no conflict of interest.

References

- Mirghiasi Z, Bakhtiari F, Darezereshki E, Esmaeilzadeh E (2014) Preparation and characterization of CaO nanoparticles from Ca(OH)₂ by direct thermal decomposition method. *J Ind Eng Chem* 20:113–117
- Liang M, Wong KL (2017) Electrical performance of epoxy resin filled with micro particles and nanoparticles. *Energy Procedia* 110:162–167
- Singha S, Thomas MJ (2008) Permittivity and tan delta characteristics of epoxy nanocomposites. *IEEE Trans Dielectr Electr Insul* 15(1):106–117
- Ngamcharussrivichai C, Meechan W, Ketcong A, Kangwansai-chon K, Butnark S (2011) Preparation of heterogeneous catalysts from limestone for transesterification of vegetable oils—effects of binder addition. *J Ind Eng Chem* 17(3):587–595
- Tang ZX, Claveau D, Corcuff R, Belkacemi K, Arul J (2008) Preparation of nano-CaO using thermal-decomposition method. *Mater Lett* 62(14):2096–2098
- Roy A, Bhattacharya J (2011) Microwave-assisted synthesis and characterization of CaO nanoparticles. *Int J Nanosci* 10(3):413–418
- Zhu Y, Wu S, Wang X (2011) Nano CaO grain characteristics and growth model under calcination. *Chem Eng J* 175:512–518
- Park HK, Bae MW, Nam IH, Kim SG (2013) Acid leaching of CaOSiO₂ resources. *J Ind Eng Chem* 19:633–639
- Assabumrungrat S, Sonthisanga P, Kiatkittipong W, Laosiripojana N, Arpornwichanop A, Soottitantawat A, Wiyaratn W, Praserttham P (2010) Thermodynamic analysis of calcium oxide assisted hydrogen production from biogas. *J Ind Eng Chem* 16:785–789
- Liu T, Zhu Y, Zhang X, Zhang T, Zhang T, Li X (2010) Synthesis and characterization of calcium hydroxide nanoparticles by hydrogen plasma-metal reaction method. *Mater Lett* 64:2575–2577
- Alavi MA, Morsali A (2010) Ultrasonic-assisted synthesis of Ca(OH)₂ and CaO nanostructures. *J Exp Nanosci* 5:93–105
- Sönmez M, Alexandrescu L, Georgescu M, Gurau FD, Ficai D, Ficai A, Trusca R, Ovidiu O, Ioana LA, Constantinescu D (2018) Influence of calcium oxide on thermal and mechanical properties of recycled polyethylene terephthalate/polyethylene mixture. In: Proceedings of the 4th world congress on new technologies (NewTech'18), Madrid, Spain. <https://doi.org/10.11159/icnfa.18.135>
- Mohamed WS, Nasr HE, Gutmann R, Sobh RA (2015) Effect of CaO nanoparticles on the properties of polyamide 6, Egypt. *J Chem* 58(3):365–375
- Sato V, Beaudoin JJ, Ramachandran VS, Mitchell LD, Tumidajski PJ (2007) Thermal decomposition of nanoparticulate Ca(OH)₂—anomalous effects. *Adv Cem Res* 19:1–7
- Ghiasi M, Malekzadeh A (2012) Synthesis of CaCO₃ nanoparticles via citrate method and sequential preparation of CaO and Ca(OH)₂ nanoparticles. *Cryst Res Technol* 47:471–478
- Surplice NA (1966) The electrical conductivity of calcium and strontium oxides. *Br J Appl Phys* 17(2):175–180
- Tangboriboon N, Kunanuruksapong R, Sirivat A (2012) Preparation and properties of calcium oxide from eggshells via calcination. *Mater Sci Pol* 30(4):313–322
- Rahman Khan MM, Wee YK, Mahmood WAK (2014) Synthesis of PANI-CaO composite nanofibers with controllable diameter and

- electrical conductivity. *Polym Compos* 36(2):359–366. <https://doi.org/10.1002/pc.22950>
19. Oskam G (2006) Metal oxide nanoparticles: synthesis, characterization and application. *Sol–Gel Sci Technol* 37:161–164
 20. Alavi MA, Morsali A (2011) Alkaline-earth metal carbonate, hydroxide and oxide nano-crystals synthesis methods, size and morphologies consideration, chapter 9. In: Masuda Y (ed) *Nanocrystal*. InTech, Rijeka, pp 237–262. <https://doi.org/10.5772/16431>
 21. Suja CP, Senthil SL, Jeyatha B, Ponmalar J, Mary K (2008) First characterization report of natural pearl of *Pinctada fucata* from Gulf of Mannar. *Biotechnol Res Innov* 2:58–62
 22. Kamba AS, Ismail M, Ibrahim TAT, Zakaria ZA (2013) Synthesis and characterisation of calcium carbonate aragonite nanocrystals from cockle shell powder (*Anadara granosa*). *J Nanomater*. <https://doi.org/10.1155/2013/398357>
 23. Tămășan M, Ozyegin LS, Oktar FN, Simon V (2013) Characterization of calcium phosphate powders originating from *Phyllacanthus imperialis* and Trochidae *Infundibulum concavus* marine shells. *Mater Sci Eng C* 33:2569–2577
 24. Stuart B (2004) *Infrared spectroscopy: fundamentals and applications*. Wiley, New York
 25. Ida H, Kawai J (2005) Portable X-ray fluorescence spectrometer with a pyroelectric X-ray generator. *X-Ray Spectrom* 34(3):225–229
 26. Nayak PS, Singh BK (2007) Instrumental characterization of clay by XRF, XRD and FTIR. *Bull Mater Sci* 30(3):235–238
 27. National Physical Laboratory (2005) Tables of physical & chemical constants. 2.3.7 thermal conductivities. Kaye & Laby Online, Version 1.0, National Physical Laboratory. www.kayelaby.npl.co.uk. Accessed 12 Oct 2018
 28. Collaboration: Authors and editors of the volumes III/17B-22A-41B (1999) Calcium oxide (CaO) dielectric constants, optical properties. In: Madelung O, Rössler U, Schulz M (eds) II–VI and I–VII compounds; semimagnetic compounds. *Landolt-Börnstein—Group III Condensed Matter (Numerical Data and Functional Relationships in Science and Technology)*, vol 41B. Springer, Berlin
 29. Von Hippel AR (1954) *Theory in dielectric materials and applications*. The MIT Press, Massachusetts, pp 3–46

Publisher's Note Springer Nature remains neutral with regard to jurisdictional claims in published maps and institutional affiliations.